EMG and Metabolite-Based Prediction of Force in Paralyzed Quadriceps Muscle Under Interrupted Stimulation

Oron Levin and Joseph Mizrahi

***Abstract*— A major issue associated with functional electrical stimulation (FES) of a paralyzed limb is the decay with time of the muscle force as a result of fatigue. A possible means to reduce fatigue during FES is by using interrupted stimulation, in which fatigue and recovery occur in sequence. In this study, we present a model which enables us to evaluate the temporal force generation capacity within the electrically activated muscle during first stimulation fatigue, i.e., when the muscle is activated from unfatigued initial conditions, and during postrest stimulation, i.e., after different given rest durations. The force history of the muscle is determined by the activation as derived from actually measured electromyogram (EMG) data, and by the metabolic fatigue function expressing the temporal changes of muscle metabolites, from existing data acquired by *in vivo* ^{31}P MR spectroscopy in terms of the inorganic phosphorus variables, Pi or $H_2PO_4^-$, and by the intracellular pH. The model was solved for supra-maximal stimulation in isometric contractions separated by rest periods, and compared to experimentally obtained measurements. EMG data were fundamental for prediction of the ascending force during its posttetanic response. On the other hand, prediction of the decaying phase of the force was possible only by means of the metabolite-based fatigue function. The prediction capability of the model was assessed by means of the error between predicted and measured force profiles. The predicted force obtained from the model in first stimulation fatigue fits well with the experimental one. In postrest stimulation fatigue, the different metabolites provided different prediction capabilities of the force, depending on the duration of the rest period. Following rest duration of 1 min, Pi provided the best prediction of force; $H_2PO_4^-$ extended the prediction capacity of the model to up to 6 min and pH provided a reliable prediction for rest durations longer than 12 min. The results presented shed light on the roles of EMG and of metabolites in prediction of the force history of a paralyzed muscle under conditions where fatigue and recovery occur in sequence.**

***Index Terms*— Electromyography (EMC), first stimulation fatigue, force history, functional electrical stimulation (FES), musculo-tendon model, metabolite-based fatigue function, postrest stimulation fatigue.**

I. Introduction

A COMMON consequence in complete paralysis is the loss of control and sensation of the body's extremities. In many cases, however, the neurons below the lesion level, as well as the muscles innervated by these nerves remain intact. If these muscles are electrically stimulated, they can be used as actuators to the paralyzed limb. In this case, electrical stimulation provides the opportunity to restore function to the stimulated muscles [1], [2].

Two major issues are associated with electrical stimulation of muscle: the mechanism of force generation by the recruitment of the muscle motor units and the decay with time of the muscle force as a result of fatigue [1], [3], [4]. Since sensory feedback from the muscle to indicate fatigue and prevent failure is missing, on-line monitoring of fatigue during activation is essential if the muscle force is to be used for feedback in closed-loop stimulation [5]. During surface FES, the synchronous mode of stimulation in which all the muscle fibers get activated simultaneously causes fatigue to occur more rapidly in the activated paralyzed limb [6]. A possible means to reduce fatigue during FES is by using interrupted stimulation [7], [8], in which fatigue and recovery occur in sequence. The history-dependency of the muscle response to FES during interrupted stimulation becomes in this case significant.

Fatigue in electrically stimulated muscles of paraplegic patients is peripheral in nature and is therefore attributed to the impairment or failure of any, or a combination of, the following processes: neuromuscular transmission, muscle action potential propagation, excitation-contraction coupling and energy metabolism [2], [9], [10]. It should be borne in mind that impairment and/ or failure of some or all of the above-mentioned processes are associated with a peripheral regulatory mechanisms which prevent the reduction of the muscle's energy reserves below their critical level [9], [11], [12]. Such regulation mechanisms incorporate susceptibility of a muscle to high frequency fatigue, which is attributed to the failure of neuromuscular transmission, action potential blocking, or low frequency fatigue which is connected to impairment of the excitation-contraction coupling mechanisms and of the rate of ATP hydrolysis [9], [11], [13]. In order to improve fatigue resistance of the muscle during FES, low-frequency stimulation (10–20 Hz) is usually used [1], [14]. In this case peripheral fatigue is thought to be further away from the neuromuscular junction, thus incorporating propagation of action potentials in the muscle membrane, excitation-contraction coupling, and creation of actin-myosin crossbridges [11]. All of the above-mentioned processes are affected by the temporal levels of intra- and extracellular metabolites and electrolytes [10], [15].

Manuscript received November 26, 1998; revised September 1999.

The authors are with the Department of Biomedical Engineering, Technion-Israel Institute of Technology, Haifa 32000, Israel. They are also with the Department of Rehabilitation Sciences, Hong Kong Polytechnic University, Hung Hom, Kowloon, Hong Kong.

Publisher Item Identifier S 1063-6528(99)07105-0.

Phosphocreatine (PCr), inorganic phosphorus (Pi), adenosinediphosphate (ADP) and intracellular pH were shown to indicate muscle force capacity during both voluntary contraction and FES [16]–[19]. The above-mentioned phosphometabolites are usually monitored by means of ^{31}P magnetic resonance (MR) spectroscopy [17], [20], [21]. Rest spectrum of ^{31}P metabolites indicates that energetically a paralyzed muscle is similar to a normal muscle. Under isometric FES as well as during the subsequent rest period, the acquired ^{31}P spectra were metabolically similar to those obtained for maximal voluntary contraction [22]. The above similarity could be expected since no injury was caused directly to the muscle cells and to the peripheral nervous system. It should be pointed out that such similarities may not exist under circumstances of muscle diseases, as some abnormalities of the rest and exhaustion spectra may emerge [23]. The decaying force and the shift of intracellular pH level in the quadriceps muscle of paraplegic subjects during FES were found to correlate to each other [17] and this correlation was used as the basis for incorporating a metabolic fatigue function into the musculotendon model of the activated muscle [6], [24]. Although intracellular pH provided good prediction for force decay during first stimulation fatigue, i.e., when the muscle is activated from unfatigued initial conditions, it failed to predict successfully force during postrest stimulation fatigue [4]. The possible reasons can be listed as follows: 1) force-pH relations may differ in first stimulation fatigue and in postrest stimulation fatigue, and 2) force may be affected more significantly by inorganic phosphorus and $H_2PO_4^-$, than by pH [16], and 3) in addition to metabolic factors, electrolytic events may be influential in governing the dynamics of fatigue and recovery [4], [10], [15], [25].

It appears that electrolytic and metabolic factors are simultaneously involved in the processes of fatigue and recovery of the muscle during FES. It was therefore concluded that a modified model, based on the simultaneous measurements of force, pH, extracellular K^+ and intracellular Na^+, should form the basis for predicting the expected force after partial recovery [2], [4]. However, no practical noninvasive means for the *in vivo* monitoring of the electrolytic history is as yet available to provide the separation ability between intra and intercellular free ions. The histories of the above-mentioned electrolytes can be correlated with fatigue and recovery via the M-wave peak-to-peak amplitude [4], [26]. Therefore, the cumulative effect of these electrolytes on the muscle force history may be incorporated into the model by means of the EMG signal.

In the present work, we established a musculoskeletal model that incorporates a fatigue-recovery algorithm, for predicting the force dynamics within the contractile element of a paralyzed muscle activated by FES. The temporal force generation capacity within the electrically activated muscle during first stimulation fatigue and postrest stimulation fatigue were estimated. In this model, the force history of the muscle is determined by the activation as driven from EMG data, and by the metabolic fatigue function expressing the temporal changes of muscle metabolites. The latter were taken from existing data acquired by *in vivo* ^{31}P MR spectroscopy [17]. When normalized to their initial, rest, values, the plotted metabolic history curves of the tests of all subjects were similar to each other and the inter subject variability was nearly eliminated [17]. During the stimulation period, the level of the above metabolites varied monotonically and correlated well with the normalized muscle force decline. Thus, although made on different subjects, the data taken from [17] can form the basis for the metabolically-based fatigue function used in our model. The force generated by the contractile element was resolved by feeding forward the measured temporal metabolic and myoelectric states of the muscle into a nonlinear model of the musculoskeletal system. The EMG M-wave signals were taken to indicate the level of neural excitation (neural input) of the muscle. The resultant muscle activation was then resolved through a first order dynamic equation of calcium extrusion and uptake from and into the sarcoplasmic reticulun (SR), and by first order reaction dynamics of calcium and troponin. The predicted decaying phase of the force and the estimated recovery index of the muscle in postrest stimulation were established by substituting the temporal changes in the levels of the muscle metabolites, including inorganic phosphorus (Pi or $H_2PO_4^-$), or intracellular pH, into a metabolic-based fatigue function. The model enables us to predict the decaying force during continuous electrical stimulation as well as the recovery capacities of the muscle after different rest periods.

II. Methodology

We modeled isometric contraction of the quadriceps muscle in the sitting position of the patient. The model was developed for the quadriceps due to the important role this muscle has in weight bearing and due to its easy accessibility for the purpose of surface stimulation, magnetic resonance (MR) spectroscopy, EMG monitoring and force calculation [4], [6], [17], [24]. An input/output diagram of our model is depicted in Fig. 1. Myoelectric (M-wave) measurements and metabolic profiles (the latter taken from existing data acquired by *in vivo*, noninvasive, ^{31}P MR spectroscopy [17]) served to evaluate, respectively, the neural excitation and metabolic history of the activated muscle, which were used further to predict the activation dynamics and the fatigue function of the contractile mechanism.

In isometric contraction, the quantity being measured is the muscle torque around a joint, from which the muscle force can be calculated [6]. It should be mentioned that during *in vivo* isometric measurements, the joint torque is determined by the combination of the average muscle-fiber length and the muscle lever arm. These anthropometric properties specify the geometry of the activated muscle and were estimated in this study by means of magnetic resonance imaging (MRI).

A. Theoretical Analysis

1) The Musculotendon Model: The most commonly used phenomenological musculotendon model consists of five elements as presented in Fig. 2 [27]. For the quadriceps, this model assumes that all the muscle fibers are parallel to each other and are oriented at the same pennation angle α,

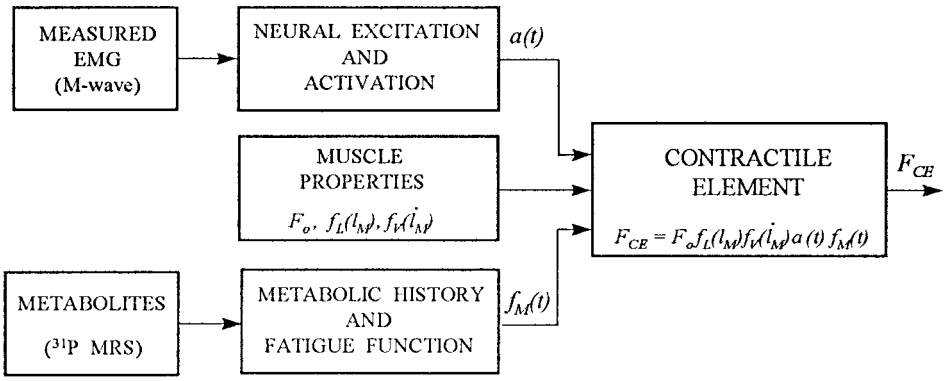

Fig. 1. Block diagram of model's inputs (measured EMG M-wave and ^{31}P spectroscopy) versus output (muscle force) of the contractile element.

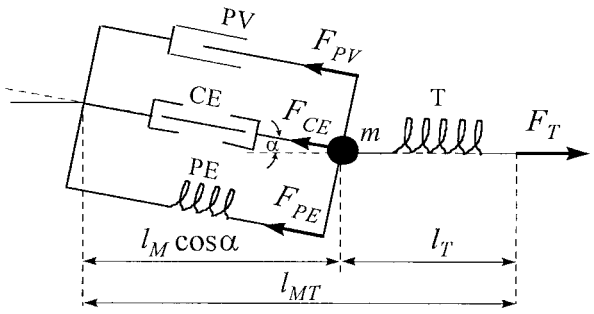

Fig. 2. Musculotendon model (PE—parallel elastic element, PV—parallel viscous damping element, CE—contractile element, T—tendon, m—muscle mass).

and that the muscle volume and cross-sectional area remain constant during isometric contraction [6], [28]. Since in our experimental work the FES electrodes were positioned over the belly of the rectus femoris, the pennation angle of this muscle head was selected to represent the quadriceps. The small pennation angle ($\alpha = 7.5°$, see [29]) of the rectus femoris head allows us to assume that, from the point of view of force projection, the line of action of the force generated by the muscle fibers is nearly parallel to the straight line connecting the origin and insertion points. Therefore, for practical calculations, this angle was assumed zero. The model includes the tendon (T) and the muscle mass (m) connected in series with three parallel elements. Two of the parallel elements are passive, representing elasticity (PE) and viscous damping (PV) of the parallel-arranged muscle fibers [6]. The forces in the tendon (F_T), the PE $(F_{\rm PE})$ and the PV $(F_{\rm PV})$ elements can be analytically represented by the following relations:

$$F_T = f_T(l_T) \quad F_{\rm PE} = f_{\rm PE}(l_M) \quad F_{\rm PV} = f_{\rm PV}\left(\dot{l}_M\right). \quad (1)$$

The variables l_T and $l_{\rm MT}$ indicate tendon length and length of the musculotendon complex, respectively. l_M represents the average muscle-fiber length $(l_M \cos\alpha = l_{\rm MT} - l_T)$. The explicit forms of f_T, $f_{\rm PE}$ and $f_{\rm PV}$ are given in Appendix A.

The third parallel component is the contractile element (CE), that represents the activated fibers in the muscle. The force $F_{\rm CE}$, in the activated contractile element was represented as the product of the following four terms: length-tension and velocity-tension relationships (explicit forms are given in Appendix A), active state and fatigue function, denoted, respectively, by the terms f_L, f_V, $a(t)$ and f_M [6], [24]. Thus,

$$F_{\rm CE} = F_o f_L(l_M) f_V(\dot{l}_M) a(t) f_M(t) \quad (2)$$

where F_o is the maximal isometric force, which is the product of the muscle's specific tension and the physiological cross-sectional area (PCSA). Equation (2) contains two general types of muscle properties: 1) specific properties, which are dependent on each subject's individual anthropometry (such as muscle mass, PCSA, length) and 2) nonspecific properties which are considered universal (such as the coefficients of the length-tension and velocity-tension relations). In paralyzed muscles isolated from voluntary control and subjected to low frequency FES, fast-twitch to slow-twitch transformation of their fibers was shown to take place [30]. Therefore, homogeneity of the fiber composition can be assumed, and lumped-parameter-modeling of the muscle becomes acceptable.

Describing the force balance equation for muscle mass m of the typical muscle (see Fig. 2), reveals

$$m\ddot{l}_M \cos\alpha = F_T - F\cos\alpha \quad (3)$$

where

$$F = F_{\rm PE} + F_{\rm PV} + F_{\rm CE}. \quad (4)$$

Upon substituting (1), (2), and (4) into (3) and rearranging, the following musculo-tendon model results:

$$\ddot{l}_M = \frac{1}{m\cos\alpha} f_T(l_T) - \frac{1}{m}[f_{\rm PE}(l_M) + f_{\rm PV}(\dot{l}_M) + F_o f_L(l_M) f_V(\dot{l}_M) a(t) f_M(t)]. \quad (5)$$

Assuming that the length-tension and velocity-tension effects remain unchanged during isometric contraction, prediction of the force generation capacity is reduced to the evaluation of the temporal states of activation and fatigue within the contractile element.

2) Excitation-Contraction Coupling and Muscle Activation: The active state $a(t)$ of the muscle fibers defines the relative amount of calcium (Ca^{+2}) bound to troponin [31], and was evaluated by substituting the muscle neural input $u(t)$, into activation dynamics model (Fig. 3). The development of tension

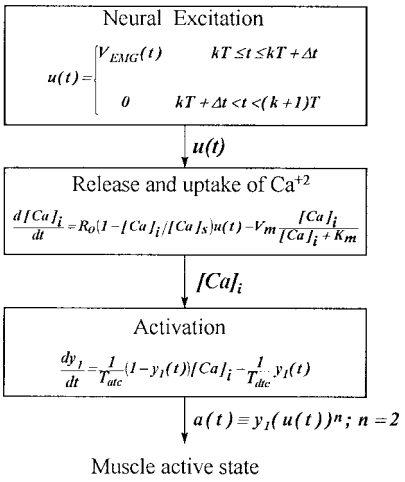

Fig. 3. Activation dynamics model. The neural excitation $u(t)$ was used to predict intracellular concentration of Ca^{+2}ions, $[Ca]_i$, resulting from the release and up-take of Ca^{+2} from and into the SR. R_o is the maximal rate of Ca^{+2} release from the SR when $u(t) = 1$. V_m is the active uptake rate constant and K_m is the SR ATPase uptake constant. The rate constants $T_{\rm atc}$ and $T_{\rm dtc}$ express respectively, the forward and backward Ca^{+2}-troponin kinetics (the latter expressing muscle active state).

in skeletal muscle involves the release of stored calcium from the sarcoplasmic-reticulum (SR) and the diffusion of calcium across the sarcomere to troponin binding sites. To describe the neural input as a function of the measured EMG, we used a tri-exponential function that expresses the time course of the envelope of the M-wave peak-to-peak amplitude $(\mathrm{EMG_{ptp}})$ [4], follows:

$$\mathrm{EMG_{ptp}}(t) = c_0[1 - c_1\exp(-t/\tau_1) - c_2\exp(-t/\tau_2)] - c_3\tanh[(t - t_3)/\tau_3]. \quad (6)$$

The first term (with τ_1) describes the rapid and tetanic response of the muscle to stimulation. The second term (with τ_2) describes the slower posttetanic potentiation due to the enhanced release of presynaptic neuro-transmitter and increased sensitivity of postsynaptic receptors, and in parallel, Ca^{+2} accumulation outside of the sarcoplasmic-reticulum [32]. The latter affects the conductivity of the potassium channels [15]. The third term (with τ_3) represents the decay phase of EMG peak-to-peak amplitude due to changes in the concentrations of the intracellular metabolites and sarcolemma electrolytes. The range and average values of the coefficients in (6) are given in Table I for both subjects in first stimulation and postrest stimulation fatigue. The data were adapted from [4].

The shape and amplitude of the EMG M-wave are affected by the propagation velocity of the action potential across the sarcolemma, the number of active muscle fibers and the amplitude of a single fiber action potential. It has been demonstrated that in the case of low frequency stimulation, as is the case with FES, the time-dependent modifications in the M-wave result primarily from the slowing down of the conduction velocity of the muscle fibers [33], [34]. On the other hand, the amplitude of a single fiber action potential shows a small percentage of change during a low frequency stimulation of either: fast fatiguing (FF) or slow oxidative (SO) muscle units [35]. On the basis of these observations,

TABLE I
AVERAGE AND RANGE VALUES OF THE COEFFICIENT IN (6) (AVERAGE GIVEN FOR FIRST STIMULATION ONLY). EMG PEAK-TO-PEAK WERE TAKEN FROM $(n = 6)$ FATIGUE TESTS MADE ON EACH SUBJECT (ADAPTED FROM [4]). AVE = AVERAGE; SD = STANDARD DEVIATION

Coefficients	First Stimulation		Post-rest Stimulation	
	Vt	Td	Vt	Td
τ_1 (sec) range	0.48 - 3.98	0.18 - 8.32	0.46 - 0.57	0.06 - 5.26
Ave (SD)	1.75 (1.29)	2.20 (2.90)		
τ_2 (sec) range	2.40 - 66.8	1.10 - 54.8	5.19 - 14.7	7.20 - 77.2
Ave (SD)	35.1 (23.3)	22.2 (16.9)		
τ_3 (sec) range	16.5 - 62.0	14.5 - 36.2	14.8 - 23.8	7.70 - 18.8
Ave (SD)	31.6 (17.6)	22.0 (7.10)		
t_3 (sec) range	2.51 - 58.9	33.2 - 54.3	40.1 - 43.6	34.4 - 42.4
Ave (SD)	40.5 (18.8)	44.1 (7.10)		
a_0 - a_3 (mV) range	0.22 - 0.97	0.60 - 3.94	1.20 - 1.64	1.70 - 4.90
Ave (SD)	0.51 (0.27)	1.20 (1.20)		

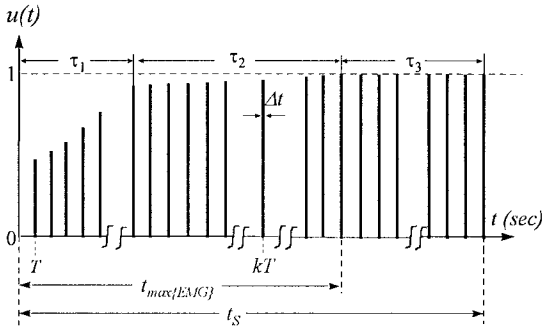

Fig. 4. Muscle neural input. τ_1, τ_2, and τ_3, are the time constants, obtained by curve-fitting the measured EMG signals as a triexponential function (6); T is the interval between two successive stimuli; t_S is the total stimulation period and k is the number of stimuli. Δt = (5 ms) is the duration of the muscle action potential.

we assumed that the amplitude of the neural input function $(V_{\rm EMG})$ of the muscle follows that of the actually measured M-wave peak-to-peak in the ascent phase of contraction, but remains unchanged afterwards. Thus,

$$V_{\rm EMG}(t) = \begin{cases} \dfrac{\mathrm{EMG_{ptp}}(t)}{\mathrm{EMG_{ptp}}(t_{\max\{\mathrm{EMG}\}})}, & 0 \le t < t_{\max\{\mathrm{EMG}\}} \\ 1, & t_{\max\{\mathrm{EMG}\}} \le t < t_S \end{cases} \quad (7)$$

where $t_{\max\{\mathrm{EMG}\}}$ designates the time at which the amplitude of the actually measured M-wave peak-to-peak reaches its maximum and t_S expresses the total duration of stimulation. To describe the neural input function $u(t)$, as a product of the EMG envelope and the stimulation frequency f, we derived the following expression:

$$u(t) = \begin{cases} V_{\rm EMG}(t), & kT \le t \le kT + \Delta t, \\ 0, & kT + \Delta t < t < (k+1)T \end{cases} \quad (8)$$

where $T\,(=f^{-1})$ is the time interval between two stimuli, k is the number of stimuli, and Δt (=5 ms) is the duration of the action-potential that is generated by each stimulus. The neural input function of the model is depicted in Fig. 4.

It was assumed, for simplicity, that the muscle contraction is limited by calcium kinetics, namely that Ca^{+2} diffusion in the

cytoplasm and acto-myosin cross-bridge formations are rapid and not acting as rate limiting factors [36]–[38]. The active state of the muscle was thus expressed by the following two dynamic variables:

a) Ca^{+2} concentration: The temporal intracellular (myoplasm) free concentration of Ca^{+2} ions, $[Ca]_i$, is governed by the release and uptake of calcium from and into the SR. The simplest assumption that one can make about calcium injection into cytoplasm is that each muscle action potential releases a fixed quantity of calcium during a certain time course [39]. Since the SR contains about five to ten times the calcium injected during the first action potential, and since experiments show a decrease in the free calcium concentration in the SR during repeated trains of electrical stimuli [37], [40], we assume that the calcium injection from the SR decreases linearly with the free calcium concentration outside the SR [39]. We used a dimensionless first-order differential equation to express the calcium kinetics within the myoplasm, as presented by (9)

$$\frac{d[\mathrm{Ca}]_i}{dt} = R_o\left(1 - \frac{[\mathrm{Ca}]_i}{[\mathrm{Ca}]_s}\right)u(t) - V_m\frac{[\mathrm{Ca}]_i}{[\mathrm{Ca}]_i + K_m} \quad (9)$$

where R_o is the maximal rate of calcium efflux from the SR into the sarcoplasm; $[\mathrm{Ca}]_s$ is the dimensionless peak of myoplasmic calcium concentration at which the gradient driving calcium injection from SR would disappear. Calcium injection from the SR in response to a single action potential is expressed by the first term in the right hand part of (9). The return of calcium from the cytoplasm to the SR was assumed, for simplicity, to result from a saturated first-order pump [37]. The uptake of calcium into the SR as consequence of SR-Ca^{+2} ATPase pumping activity is given by the second term in the right hand part of (9). Note that $0 < [\mathrm{Ca}]_i/[\mathrm{Ca}]_s < 1$ at any given time. V_m and K_m express, respectively, the maximum rate of calcium uptake by the SR-Ca^{+2} ATPase pump and the dimensionless intracellular calcium concentration in which half-maximal pump rate occurs.

b) Active state of the muscle: The active state of the muscle, $a(t)$, is governed by $[\mathrm{Ca}]_i$. Full activation (i.e., $a = 1$) will occur when the maximal number of cross-bridges results from the interaction between Ca^{+2} and troponin [6]. We assume: 1) that Ca^{+2} ions bind independently to troponin, 2) troponin releases its inhibition over the actin binding sites only after it has bound two calcium ions, and 3) when the troponin-mediated inhibition is removed, myosin is free to bind actin. Let $y_0(t)$ be the fraction of regulatory sites on troponin without a Ca^{+2} bound, and let $y_1(t)$ be the fraction of troponin sites with Ca^{+2} bound (note that $y_0 + y_1 = 1$). If there is no cooperativity between the sites, then the reaction between calcium and troponin is modeled by the following first-order reaction [38]:

$$y_0 \underset{T_{\mathrm{dtc}}}{\overset{[\mathrm{Ca}]_i T_{\mathrm{atc}}}{\rightleftarrows}} y_1 \quad (10)$$

given by the differential equation:

$$\frac{dy_1}{dt} = \frac{1}{T_{\mathrm{atc}}}(1 - y_1(t))[\mathrm{Ca}]_i - \frac{1}{T_{\mathrm{dtc}}}y_1(t). \quad (11)$$

TABLE II
SUMMARY OF THE COEFFICIENTS IN THE EXCITATION-CONTRACTION MODEL [(9) AND (11)]

Coefficient	How Determined	Description
R_o = 74.54 [sec^{-1}]	estimated	maximum rate of calcium efflux from SR
$[Ca]_s$ = 1	assumed	dimensionless peak of myoplasmic calcium concentration.
V_{max} = 4 [sec^{-1}]	Ref. [41]	maximum rate of calcium uptake by SR.
K_m = 0.0055	Ref. [41]	dimensionless calcium concentration at half maximum uptake rate by SR
T_{atc} = 0.012 [sec]	Ref. [42]	calcium-troponin attachment time constant
T_{dtc} = 0.2 [sec]	Ref. [42]	calcium-troponin detachment time constant

The rate constants T_{atc} and T_{dtc} express respectively, the forward and backward Ca^{+2}-troponin kinetics [37], [38]. It was shown that force production is proportional to the number of Ca^{+2} ions (n) bound to each troponin molecule [38], hence, $F_{\mathrm{CE}} \propto y_1^n$, and $a(t) \equiv y_1(u(t))^n$ with $n = 2$. The parameters used in (9) and (11) are given in Table II [41], [42].

3) Fatigue-Recovery Model: The fatigue function, denoted by $f_M(t)$, is determined by the history of the muscle metabolites and by force-metabolites relations (Fig. 5). It defines the temporal force producing capacity of the activated muscle fibers as a function of their metabolic history profiles [6], [24]. It was shown that in the presence of fatigue during prolonged FES, substantial changes take place in the levels of intracellular metabolites such as Phosphocreatine (PCr), inorganic phosphorus (Pi) and pH in parallel to the decrease in the mechanical output of the muscle [17]. The metabolic history of the contractile element, taken from existing data acquired by ^{31}P MR spectroscopy [17], includes the changing levels of the above-mentioned metabolites from their rest values during the stimulated contraction and during the following rest period. The procedure used to predict the fatigue state of the muscle during interrupted stimulation is depicted in Fig. 5, and described below.

The metabolic parameters of the muscle were expressed in terms of the temporal shift of the peaks of the acquired ^{31}P-MR spectra during stimulation and during the following rest period [17]. Specifically, the measured metabolic parameters included: 1) the decrease of PCr and increase of Pi from the unfatigued rest values and 2) the pH-dependent chemical shift of the Pi peak relative to the pH-independent PCr reference. The above mentioned parameters were used further to calculate the histories and asymptotic values of pH, Pi and $H_2PO_4^-$ [16], [17]. The full derivation is demonstrated in Appendix B.

During interrupted stimulation, fatigue and recovery occur alternately. The histories of the above-mentioned metabolites must therefore be expressed in terms of two time-dependent metabolic functions, one for fatigue and one for rest. The procedure of concatenating fatigue and recovery curves is illustrated in Fig. 6 for the level $x(t)$ of an arbitrary metabolite $X \equiv \{\mathrm{pH}, \text{ or } \mathrm{Pi}, \text{ or } H_2PO_4^-\}$. The first cycle of intermittent stimulation starts with the rest metabolic level x_0 at time t_0, (point 1 in Fig. 6). In the first stimulation (FS), i.e.

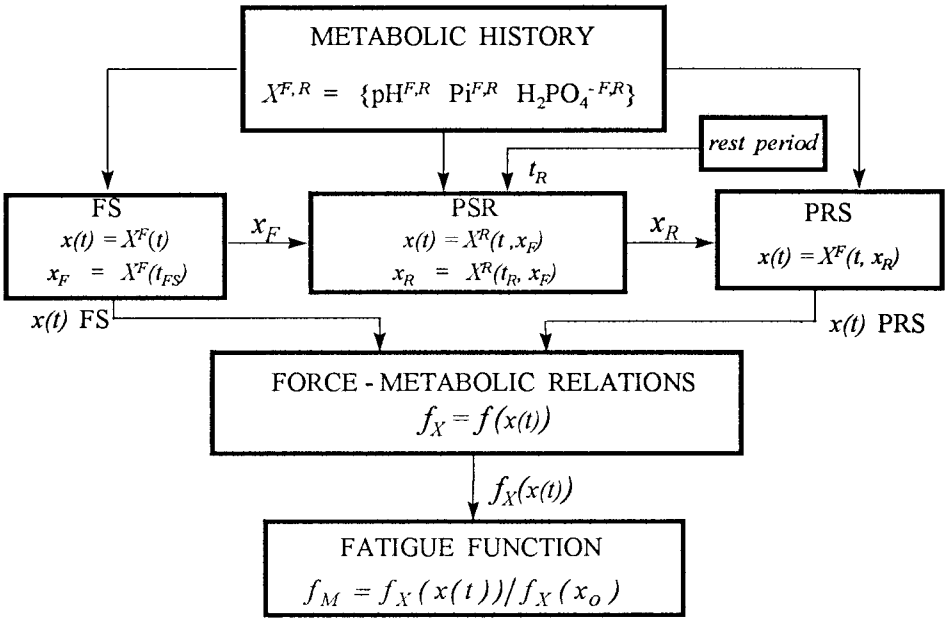

Fig. 5. Fatigue function $f_M(t)$ as obtained by substituting the metabolic state $x(t)$ of the measured metabolic history into the model. The functions X^F and X^R express, respectively, the variation of the metabolite X (=pH, or Pi or $H_2PO_4^-$) from its rest value x_0 during the first stimulation (FS), postrest stimulation (PRS), and during the poststimulation rest (PSR) phases. x_F and x_R express, respectively, the metabolic actual levels at the end of the stimulation and the rest periods. $t_{\rm FS}$, t_R and $t_{\rm PRS}$ are, respectively, the time periods of the first stimulation, poststimulation rest, and postrest stimulation.

when the muscle is activated from a previously unfatigued conditions, the level $x(t)$ of the metabolite X, varies according to the fatigue function $X^F(t)$, along the curve connecting points 1 and 2 [Fig. 6(a)]. When stimulation is stopped (poststimulation rest—PSR), the level $x(t)$ of the metabolite X begins its recovery period and varies according to the function $X^R(t, x_F)$, along the curve connecting points 3 and 6 [Fig. 6(b)]. Recovery of the metabolite starts from the latest value reached during stimulation, denoted by $x_F = X^F(t_{\rm FS})$ (point 2), where $t_{\rm FS}$ expresses the duration of first stimulation. Likewise, during the postrest stimulation (PRS) the level $x(t)$ of the metabolite X varies according to the function $X^F(t, x_R)$, along the curve connecting points 5 and 6 (Fig. 6(a)). In the PRS $x(t)$ will start its fatigue phase from the latest value, $x_R = X^R(t_R, x_F)$, that was reached during the poststimulation rest period t_R (point 4). The history of each metabolite during first and postrest stimulation [Fig. 6(c)] can thus be described as shown in (12) at the bottom of the page.

Force metabolite relations were established for first stimulation fatigue by curve-fitting of the measured (normalized) force with the corresponding profiles of phosphometabolites [6], as shown in (13) at the bottom of the page. The above presentation with the coefficients given in Table III were used to predict the muscle force capacity during first and postrest stimulation contractions. Equation (13) was normalized with respect to f_X corresponding to the metabolic level of the unfatigued state of the muscle, where the force output is found to be the highest. A normalized metabolic fatigue function f_M is thus obtained, incorporating the metabolic history of the muscle during first stimulation fatigue and postrest stimulation fatigue, as follows:

$$f_M(x(t)) = \frac{f_X(x(t))}{f_X(x_o)} \tag{14}$$

where x_o denotes the initial metabolite level, in the unfatigued condition.

Note that $0 < f_M\ (x(t)) < 1$ at any given time.

4) Computation Formulation: The musculotendon model and the excitation-contraction model were combined together to form the global model governing the force dynamics of the activated muscle. The components of the state vector $\mathbf{z}(t) = [z_1(t),\ z_2(t),\ z_3(t),\ z_4(t)]^T$ carrying the dependent variables of the vector differential equation are established as

$$x(t) = \begin{cases} X^F(t); & 0 < t < t_{\rm FS} \\ X^F(t, X^R(t_R, X^F(t_{\rm FS}))); & (t_{\rm FS} + t_R) < t < (t_{\rm FS} + t_R + t_{\rm PRS}). \end{cases} \tag{12}$$

$$f_X = \begin{cases} b_1(1 - \exp[b_2(x(t) - b_3)]) + b_4[x(t) - b_5]; & x(t) \equiv {\rm pH}(t) \\ d_1 - d_2 \tanh[d_3(x(t) - d_4)]; & x(t) = \{{\rm Pi}(t), {\rm H_2PO_4^-}(t)\}. \end{cases} \tag{13}$$

TABLE III
AVERAGE AND RANGE VALUES OF THE COEFFICIENTS IN THE FATIGUE FUNCTION (13) AS WERE ESTIMATED BY CURVE-FITTING OF THE FORCE OUTPUT WITH THE METABOLIC HISTORY OF pH, Pi AND $H_2PO_4^-$ DURING THE FIRST STIMULATION. DATA RELATED TO ($n = 7$) FATIGUE TESTS MADE ON BOTH SUBJECTS. IN (13), $b_4 < 0.0001$ AND $b_5 = 7.2$ (REST LEVEL OF pH)

	pH			Pi				$H_2PO_4^-$			
	b_1	b_2	b_3	d_1	d_2	d_3	d_4	d_1	d_2	d_3	d_4
Min value	0.995	- 4.86	6.13	0.429	0.383	1.057	3.13	0.496	0.285	0.418	8.61
Max value	1.026	- 6.92	6.16	0.602	0.611	3.41	3.44	0.671	0.474	0.673	9.23
Average	0.998	- 5.83	6.15	0.545	0.444	2.53	3.24	0.557	0.409	0.525	9.00
(SD)	(0.019)	(0.90)	(0.01)	(0.068)	(0.094)	(0.88)	(0.12)	(0.072)	0.073)	(0.108)	(0.24)

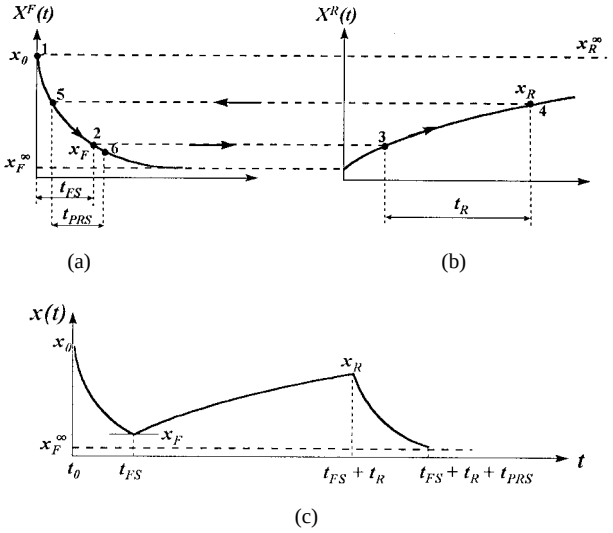

Fig. 6. (a) The function $X^F(t)$ indicating the metabolic level $x(t)$ during: first stimulation (FS), denoted by the subinterval 1–2; and postrest stimulation (PRS), denoted by the subinterval 5–6. (b) The function $X^R(t)$ indicating the metabolic level $x(t)$ during recovery. (c) The metabolic history of the metabolite X during FS, post stimulation rest (PSR) and PRS. x_F^∞ and x_R^∞ represent, respectively, the values of $x(t)$ at full exhaustion, and after a full recovery.

follows. Define

$$z_1 \equiv l_M(t) \quad z_2 \equiv \dot{l}_M(t) \quad z_3(t) \equiv [\mathrm{Ca}]_i \quad z_4(t) \equiv y_1(t). \tag{15}$$

The time derivatives of these components are designated as

$$\begin{aligned} \dot{z}_1(t) &= z_2(t) \\ \dot{z}_2(t) &= f_1(z_1(t), z_2(t), z_3(t), z_4(t)) \\ \dot{z}_3(t) &= f_2(z_3(t), u(t)) \\ \dot{z}_4(t) &= f_3(z_3(t), z_4(t)). \end{aligned} \tag{16}$$

The functions f_1, f_2 and f_3 represent, respectively, the right hand parts of (5), (9), and (11).

Equation (16) was resolved by using Runge–Kutta numerical integration methods. Rest conditions and values for the nonspecific muscle parameters were taken from previous works [6], [24], [43]. Rate constants and physiological parameters for the excitation-contraction mechanism were taken from given experimental data on calcium kinetics in skeletal muscle [36]–[38], [42], [44]. Note that the initial fiber length, $z_1(0)$ that corresponds with the steady state solution at a certain knee angle was obtained by solving (5) in which the initial values $\mathbf{z}(0)$ were substituted.

5) Sensitivity Analysis: A sensitivity analysis of the coefficients of the metabolically based fatigue functions (13) was performed due to their important role in controlling the fatigue profiles of the muscle during both first and postrest stimulation sessions. This allowed us to characterize the model sensitivity to the expected variability of the coefficients summarized in Table III, including: b_1, b_2, b_3 (of the pH-dependent fatigue function) and d_1, d_2, d_3, d_4 (of the Pi/$H_2PO_4^-$-dependent fatigue function). Of the above listed coefficients b_1 was found to negligibly affect the prediction capacity of force (<0.1% for 10% variation of b_1). Variation of the other coefficients affected mostly the descending phase of contraction, when fatigue was rather substantial. One (SD) increase (in accordance with the data presented in Table III) varied the expected peak force by less than 1%. In the decaying phase of contraction a similar perturbation caused the expected force to change in the range from 2 to 22%, at $t = 60$ s from the onset of stimulation, and from 8.5 to 36%, at $t = 150$ s from the onset of stimulation.

B. Experimental Procedure and Data Acquisition

1) Measurements of Torque and EMG: The fatigue of the right quadriceps muscles of paraplegic subject was studied isometrically at a knee flexion angle of 60°. Two subjects, Vt and Td, aged 21 years old when FES was first applied, and with levels of injury at T4 and T6–7, respectively, took part in the measurements. Transcutaneous stimulation was provided from an adjustable electrical stimulator [45], providing monophasic rectangular pulse trains, with parameter values as follows: frequency 20 Hz, pulse width 0.25 ms and intensity of up to 200 mA. For the studied subjects, the current intensities for supramaximal stimulation were 100 mA (Vt) and 70 mA (Td). This latter parameter was determined for each subject from his isometric recruitment curve, as the current above which the force curve levelled off. Each test included two contractions, one of 180 sec and one of 100 sec, separated by rest periods of 3, 6, 12, 15 and 18 min. For subject Vt an additional rest period of 1 min was included. On each testing day, the FES sessions were made before any electrically induced activity (e.g., training) took place. All fatigue tests were made with the same stimulation parameters. The rest durations between the first (primary) and postrest stimulations differed, however, from test to test.

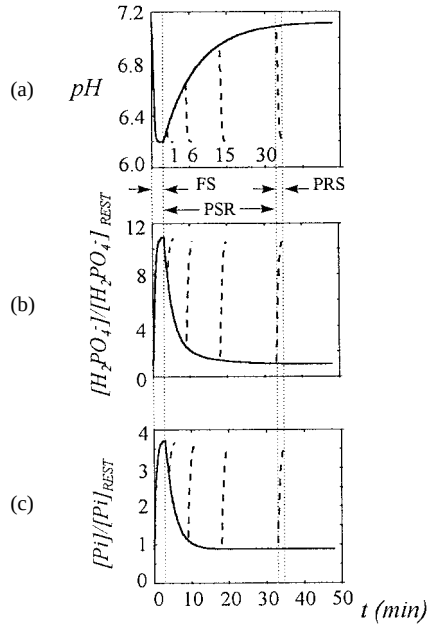

Fig. 7. The metabolic levels used as inputs in our model: (a) pH, (b) $H_2PO_4^-$, and (c) Pi during first stimulation (solid line), and post rest stimulation (doted line), following 1, 6, 15, and 30 min of rest. The metabolic levels of $H_2PO_4^-$ and Pi were normalized to their rest values.

The knee joint torque (M_k) and the surface EMG (M-wave signal) of the quadriceps muscles were recorded simultaneously. M_k was measured by an especially designed load cell, attached to an adjustable testing chair [3]. The quadriceps tendon force was calculated from the measured knee torque by resolving the static equilibrium equations of the knee's tibio-femoral and patello-femoral joints [3].

The M-wave was recorded by three 10-mm diameter gold cup-electrodes: two active and one for reference. The active electrodes were placed 2 cm apart and aligned with the FES electrodes halfway between them and were connected to a specially designed 10 kHz bandwidth dc amplifier with stimulus artifact suppression [26]. The reference electrode was placed on the antero-lateral surface of the shank, 10 mm below the level of the patellar tendon.

2) Evaluation of Intracellular Metabolic Modifications During Fatigue and Recovery: The metabolic input of the model including the time dependent metabolic shift of pH, and inorganic phosphorus (Pi and $H_2PO_4^-$) is depicted in Fig. 7. The curves describing the metabolic history were taken from existing data acquired by noninvasive, *in vivo*, ^{31}P MR spectroscopy during 3 min first stimulation, when the muscle is activated from an unfatigued initial conditions and during the following 45-min poststimulation rest period [17], [46]. The dashed lines describe the time course of each of the metabolites during postrest stimulation, after rest period of different durations. The procedure of concatenating fatigue and recovery curves is illustrated in Fig. 6.

III. Results

1) Excitation-Contraction Coupling and Muscle Activation: The estimated patterns of the intracellular calcium concentrations $[Ca]_i$, muscle activation $a(t)$ and the quadriceps tendon force F_T are demonstrated in Fig. 8 for the first stimulation fatigue. The results presented in Fig. 8 were obtained by substituting the neural excitation function $u(t)$ that is presented in Fig. 4 into our activation dynamics model (Fig. 3). The dimensionless concentration of calcium ions in the myoplasm exhibits a continued increase similar to that measured experimentally by means of aequorin responses [40]. During its rapid ascent phase, the build-up of the predicted force was slower compared to the build-up of the measured force. However, a good agreement between the two sets of curves, predicted and measured force trajectories was achieved after the first second of stimulation.

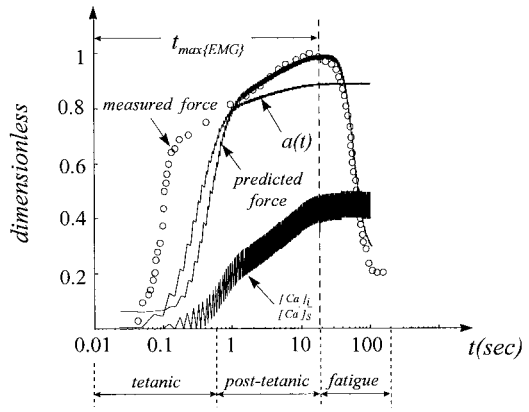

Fig. 8. Model prediction of the muscle force and the measured force for the dimensionless intracellular calcium concentrations $[Ca]_i/[Ca]_S$, and the activation $a(t)$, as obtained by substituting the muscle neural input $u(t)$, into the activation dynamics model.

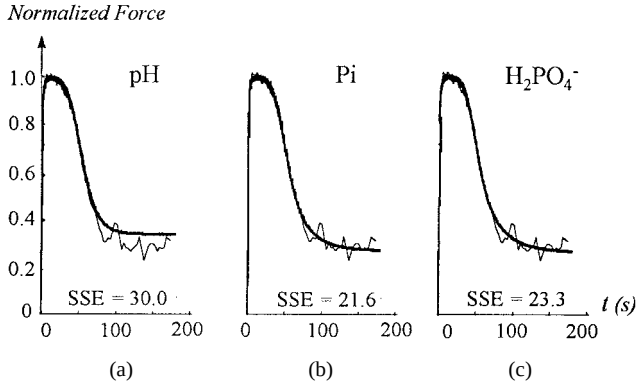

Fig. 9. First stimulation fatigue: predicted (bolded) and measured (solid) force profiles obtained when the EMG together with metabolic history of (a) pH, (b) Pi, and (c) $H_2PO_4^-$ served as input of the model. Average SSE values between the predicted and measured force profiles are given.

2) Predicted Fatigue Trajectories During First Stimulation: Typical fatigue curves of the quadriceps force as predicted from our model, together with the experimentally measured force are shown in Fig. 9 for first stimulation. Mean values and standard deviations were obtained from data collected over first stimulation fatigue tests for the two subjects ($n = 7$). The sum of the squared errors (SSE) between the predicted and the measured force profiles was used to compare to goodness of fit between these profiles. Good agreement between the two sets of curves; predicted (bolded curve) and measured (solid curve), was obtained for the first stimulation when the

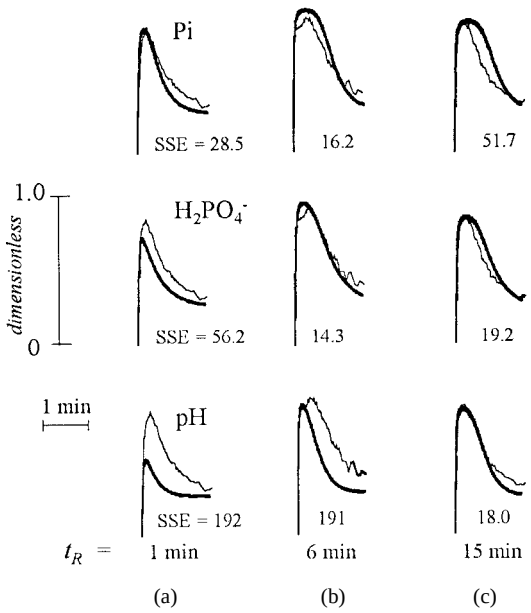

Fig. 10. Postrest stimulation fatigue: predicted (bolded) and measured (solid) force profiles as obtained for postrest session following rest durations of (a) 1 min, (b) 6 min, and (c) 15 min. SSE values between the predicted and measured force profiles are given.

TABLE IV
THE SUM OF THE SQUARED ERRORS (SSE) BETWEEN PREDICTED AND MEASURED FATIGUE CURVES IN POSTREST STIMULATION FATIGUE, AS OBTAINED FOR EACH METABOLIC INPUT AT DIFFERENT REST PERIODS

Rest period [min]	1	3	6	12	15	18
Pi	28.5	88.7	16.2	36.0	51.7	61.9
$H_2PO_4^-$	56.2	70.6	14.3	13.6	19.2	29.4
pH	192	203	192	49.7	18.0	17.6

EMG peak-to-peak together with the history of the inorganic phosphorus, either Pi $(\text{SSE} = 21.6 \pm 11.0)$ or $H_2PO_4^-$ $(\text{SSE} = 23.3 \pm 11.5)$, served as inputs of the model. Somewhat poorer agreement $(\text{SSE} = 30.0 \pm 23.0)$ between predicted and measured curves of fatigue was obtained when the history of pH served as the model's metabolic input.

3) Predicted Fatigue Trajectories during the Postrest Stimulation: Fig. 10 depicts the predicted (bolded) and measured (solid) curves of the quadriceps force, as obtained for postrest sessions, following rest durations of 1, 6 and 15 min. Both predicted and measured force histories that were obtained during the postrest sessions were normalized to their respective maxima which were obtained in the first stimulation sessions. The results obtained, present different prediction capacities of the model, in accordance with the selected metabolic input. For a short period of rest (1 min), Pi $(\text{SSE} = 28.5)$ provided a good agreement between predicted and measured force, as opposed to $H_2PO_4^-$ $(\text{SSE} = 56.2)$ and pH $(\text{SSE} = 192)$. After 6 min of rest, good predictability was obtained when using $H_2PO_4^-$ $(\text{SSE} = 14.3)$ Finally, for a long period of rest (15 min) the optimal prediction was obtained by using the pH history $(\text{SSE} = 18.0)$. Table IV summarizes the obtained SSE values between the predicted and measured fatigue trajectories in the postrest stimulation, for the model's selected metabolic inputs, at different rest periods.

IV. DISCUSSION

The central issue in the present study was to develop a musculotendon model by which the force history of an electrically stimulated paralyzed muscle can be predicted. The measured myoelectric signals and the metabolic histories were fed into an extended musculoskeletal model which was used to predict muscle force history following fatigue and recovery. Based on our previous metabolic curves during fatigue, we established a fatigue-recovery algorithm governing the muscle force history within the contractile element. The fatigue tests made repetitively on each of the subjects, allowed us to validate experimental parameters such as the coefficients of the metabolically based fatigue function (Table III). The model presents reliable prediction of force history due to metabolic history for all the tested metabolites during first stimulation fatigue. In postrest stimulation, different metabolites provide a reliable prediction of the force in different resting periods.

The artificial activation of the human musculoskeletal system, as may be required in the locomotion of paralyzed subjects, relies on the ability to predict and control the forces and torques produced by the electrically stimulated muscles. Predictability of the force variations under the circumstances of fatigue and recovery could provide the basis for a feedforward controller to determine the muscle stimulation patterns that would compensate for force loss and enable completion of desired tasks. In addition, the estimated force profiles could be used to compensate for the absence of the natural sensory feedback from the paralyzed limbs and to indicate force generation capacity of the electrically stimulated muscles.

As supramaximal FES is analogous to maximal voluntary contraction (MVC), the principles discussed in this model could be applied to model force prediction in peripheral fatigue/recovery in normal subjects. Experimental work would however be necessary to validate this approach.

A major difficulty in such a model lies upon the fact that the dynamics of the contractile mechanism incorporates a wide set of state variables and an inherent nonlinearity. In our previous models of a fatiguing muscle force dynamics, these state variables incorporated the length, the contraction velocity and the activation of the muscle, and metabolite-based fatigue function [6]. However, as has been pointed out, calcium extrusion and uptake as well as the interactions between calcium and troponin (the latter determines the stiffness of the contractile mechanism) are affected by the transitions of extra- and intracellular concentrations of electrolytes and metabolites from their rest level [10], [15], [44]. Practically, monitoring of intracellular calcium concentration, calcium kinetics or the contractile tissue stiffness is not feasible *in vivo*, thus validation of the present model was restricted to the force generation capacity of the muscle.

During its rising phase, the force build-up involved two time constants which describe a rapid, tetanic ascent phase preceding a slower build-up of the muscle force due to posttetanic potentiation. A parallel behavior of two time-constant

ascending phases, was observed for the M-wave peak-to-peak envelope. However, the build-up rate of the force during its rapid ascent was considerably faster (0.61 ± 0.42 s for subject Vt and 0.28 ± 0.15 s for subject Td) than the ascent of the M-wave peak-to-peak envelope (1.75 ± 1.29 s and 2.20 ± 2.90 s [4]). In this model, the ascending rate of the predicted force is dominated by the muscle neural input, i.e., by the ascending rate of the M-wave envelope. Otherwise, both the predicted and the measured curves of the muscle force dynamics demonstrated a parallel ascending course during the posttetanic response phase (Fig. 8). This behavior is in accordance with previously published values of the slow time constants of both the force (35.7 ± 29.9 s for subject Vt and 31.0 ± 17.5 s for subject Td) and the M-wave peak-to-peak envelope (35.1 ± 23.3 sand 22.2 ± 16.4 s, respectively, [4]). It should be mentioned that the predicted force profiles depicted in Figs. 8–10 were obtained by assuming: 1) that the muscle neural input follows the M-wave peak-to-peak envelope in its ascending phase and levels off thereafter and 2) that the decaying phase of the force is attributed exclusively to the metabolite-based fatigue function.

Metabolic history was measured via ^{31}P MR spectroscopy, incorporating the temporal levels of Pi, pH and $H_2PO_4^-$, each of which was used independently of the others to express the force generation capacity of the contractile element. This was accomplished by defining a force-metabolic fatigue function (13), which was obtained from curve-fitting of the measured force output versus the corresponding metabolic variable. Incorporating the history of Pi into our model provides a reliable prediction for the force capacity during postrest stimulation fatigue following a rest duration of 1 min. Pi, however, fails to predict the mechanical output when the rest duration exceeds 3 min. The history of $H_2PO_4^-$ extends the prediction capacity in our model to up to 6 min. Incorporating the pH history provides a reliable prediction of force capacity for rest durations longer than 12 min, but fails to do so for short periods of rest. The results thus presented, indicate that the force/recovery kinetics may involve at least two time scales, each governed by a different metabolic process.

During rest, rate of recovery of the Pi peak in an electrically evoked contraction of a paralyzed muscle was reported to be the fastest ($t_{1/2} = 1.6$ min); followed by the relatively slower ($t_{1/2} = 5.8$ min) resynthesis of the PCr [17]. The fast recovery of Pi in short rest durations (i.e., $t_r < 3$ min) was explained by its quick reuse to synthesize PCr via mitochondrial oxidative phosphorylation [20], [47]. Resynthesis of PCr is accompanied by extensive proton production [21], [47]. Thus at this stage, intracellular concentrations of the hydrogen ions (H^+) is expected to be far from its unfatigued level. We therefore suggest that at the early stage of recovery, transport of Pi across the inner mitochondrial membrane reduces Pi concentration at the vicinity of the contractile proteins, thus enhancing the force production capacity of the muscle. The fast phase of Pi recovery is followed by a very slow disappearance of the inorganic phosphorus. This stage of recovery is attributed to the slow uptake of Pi into the glycolytic fibers [47]. At this stage of recovery, force generation capacity is best predicted by incorporating the history of $H_2PO_4^-$ into our model. Since the recovery of both Pi and $H_2PO_4^-$ is accompanied by an extensive production of protons [20], recovery of the pH is expected to be the slowest and accomplished mostly by secondary active transpose mechanisms [20]. This is in accordance with the ability of previous models [6], [24] and the present model to predict the muscle force generation capacity due to pH only at the last stages of recovery.

The pH dependent fatigue function predicts that the muscle restores its mechanical output up to full recovery after rest duration of 30 min [24]. Force measurements reveal, however, that after similar rest duration the peak force that was obtained during the second FES contraction (postrest stimulation) approached only 85 to 90% of the maximal force achieved during the first (primary) contraction [48]. In the present model, the intracellular pH history was derived from the chemical shift of the Pi peak relative to the PCr peak. During heavy exercise, Pi appears in two different pH peaks, where the high-pH Pi peak corresponds to the oxidative muscle fibers and the low-pH Pi peak corresponds to the glycolytic fibers. During recovery, the high-pH Pi peak decreases rapidly and disappears within 20–40 sec after cessation of the contraction, while the low-pH peak decreases gradually with a concomitant, very slow rise in pH [47]. Yoshida and his colleagues [47] suggested that the rate of disappearance of the Pi peak corresponding to the low-pH during recovery depends upon the oxidative capacity of the glycolytic fibers, and that this capacity is suppressed at low pH. Hence, the slow disappearance of the low-pH Pi peak during recovery may be a manifestation of the suppression of glycolysis at low pH, resulting from the accumulation of either lactate or H^+ ions in the glycolytic muscle fibers. Contrary to the ability to detect the shift of the intracellular H^+ concentration *in vivo* by means of ^{31}P MR spectroscopy (as expressed in the existing metabolic data), the concentration of lactate can not be detected noninvasively. We therefore suggest that the metabolic profiles taken from existing data acquired by noninvasive, *in vivo*, ^{31}P MR spectroscopy measurements would provide reliable prediction capacity for muscle recovery within a specific boundaries of rest durations which incorporates the slow disappearance of the low-pH Pi peak.

Electrolytic factors were found to be significant in governing the muscle's membrane rest potential and action potential as well as the excitation-contraction coupling [15], [25]. Accordingly, it was initially suggested that the cumulative effect of the above-mentioned electrolytes on the muscle force history can be incorporated into a fatigue-recovery model via the measured EMG signal [2]. It should be pointed out, however, that the surface EMG M-wave signal provides reliable data on the muscle neural input only if the changes versus time of both the M-wave peak-to-peak amplitude and the depolarization magnitude of the sarcolemma action potentials exhibit a similar course. We suggest that for a fatiguing muscle, the increased conduction velocity of the measured compound muscle action potential, and the increased conduction velocity standard deviation would provide an erroneous interpretation for muscle neural input during the decaying phase [49]–[51]. Accordingly, the measured surface M-wave provide a reliable data on the muscle neural excitation, only during its ascending phase while the sarcolemma is not yet fatigued. Since the

recovery of the sarcolemma lasted from 1 to 3 min, it is feasible to use the measured M-wave peak-to-peak amplitude as predictor for neural excitation at the postrest stimulation as well.

V. Conclusion

We have developed a musculo-tendon model for the electrically activated muscle of paraplegic subjects under conditions of interrupted FES. The activation dynamics and the fatigue function of the contractile element were incorporated into the model to comply with the experimentally observed changes in myoelectric and metabolic parameters. The model was formulated to allow quadriceps muscle force prediction under general dynamic activation conditions including first stimulation fatigue and postrest stimulation fatigue, separated by various rest periods. The model was solved for supramaximal stimulation in isometric activation and compared to experimentally obtained measurements. The model presents different roles for EMG and metabolites in predicting the force profiles of the electrically stimulated paralyzed muscle. EMG data provide reliable prediction for the ascending phase of the force during the posttetanic response of the muscle. On the other hand, prediction of the decaying phase of force is possible only by means of a metabolite-based fatigue function. The predicted force obtained from the model in first stimulation fatigue fits well with the experimentally measured. In postrest stimulation fatigue, the model presents different prediction capacities of force in accordance with the selected metabolic input. It is believed that learning the dynamic model of the muscle will enable to design a strategy for reducing the muscle fatigue during FES. Additionally, the task of the feedback controller becomes simplified, since the feedback errors can be estimated and reduced. This model can provide the basis to a reference-based open-loop controller by which the stimulation patterns are precomputed to fulfil the motor task requirements. Additionally, or alternatively, this model can provide the basis for a closed-loop, computed-torque controller to increase stability during standing or walking by means of an FES system.

Appendix A
Equations and Parameters Values of the Musculo-Tendon Elements

1) Musculo-Tendon Passive Elements: The fragment of the five-element model that corresponds to the muscle tendon (T) is represented by a nonlinear spring for which the length-tension relationship is subdivided into two components: 1) an exponential relationship for shorter lengths and 2) a linear relationship for the longer lengths. Following Zajac [52], we can write:

$$F_T = f_T(l_T) = \begin{cases} \sigma_T A_T[\exp\{k_{\rm TE}(l_T - l_{T0})\} - 1], & l_{T0} \le l_T \le l_{TC} \\ k_T(l_T - l_{TC}) + F_C, & l_T > l_{TC} \end{cases} \quad \text{(A.1)}$$

where F_T is tendon force, l_T is tendon length, l_{T0} is tendon length at rest, l_{TC} is the tendon length at which the tendon tension shifts from a nonlinear to a linear curve, and F_C is the tendon force corresponds to the tendon length l_{TC}. σ_T, $k_{\rm TE}$, and k_T are stiffness constants, and A_T is the tendon cross-section area.

The muscle itself was subdivided into a passive and active components, including two parallel elastic (PE) and parallel viscous (PV) elements. The active-contractile element is discussed in Appendix A2). The PE—parallel elastic element is represented by a nonlinear spring, where the passive stretch of the muscle produces an increase of force with increasing length. It was indicated that the passive muscle fiber force increases exponentially with respect to the fiber length l_M [52], thus

$$F_{\rm PE} = f_{\rm PE}(l_M) = F_{PO}[\exp\{k_{\rm PE}(l_M - l_{M0})\} - 1] \quad \text{(A.2)}$$

where l_{M0} is the length of the fiber at rest, F_{PO} is the force corresponds with l_{M0}, and $k_{\rm PE}$ is a stiffness coefficient. The PV—parallel viscous element, which represents the damping force $F_{\rm PV}$ due to the viscous muscle fluids has been found proportional to the rate of change of the muscle's length [6], and is represented by

$$F_{\rm PV} = f_{\rm PV}(\dot{l}_M) = -k_D \dot{l}_M \quad \text{(A.3)}$$

where k_D is the coefficient of viscous friction, and $\dot{l}_M$ is the rate of change in the muscle fiber length.

2) The Contractile Element: We refer the reader to the model's input versus output diagram of the active contractile element, as shown in Fig. 1. The force produced by the active contractile element is dependent upon the muscle fiber length (l_M), the muscle contraction velocity, determined by the rate of change of the muscle fiber length $(\dot{l}_M)$, the level of the muscle active state and the muscle fatigue. Modeling of the muscle activation and the muscle fatigue function as determined respectively from the muscle neural excitation and the muscle metabolic history is discussed in detail in the body of our manuscript. The relationship between muscle length and muscle active force at zero velocity, as taken from the literature [43], and presenting an average effect of all fiber lengths on the muscle force, follows:

$$f_L(l_M) = \sin(b_1(l_M/l_o)^2 + b_2(l_M/l_o) + b_3) \quad \text{(A.4)}$$

where l_o is the muscle length at which the maximal isometric force is achieved and b_i $(i = 1, 2, 3)$ are curve fitting constants that were adapted from the literature [6]. At short lengths (i.e., $l_M \approx 0.5 l_o$), actin filaments can overlap and interfere with one another, thereby reducing the amount of potential interaction between the myosin cross-bridges and the actin attachment sites. At intermediate lengths (i.e., $l_M \approx l_o$), interaction between the myosin cross-bridges and actin attachment sites is maximal. This intersection then reduces with increasing length (i.e., $l_M > l_o$) until the force drops to zero when the two filaments (the actin and the myosin) no longer overlap.

The modified velocity-tension relationship in the contractile element describes the fiber tension as a function of the shortening or lengthening velocities. This relationship is given by the following equation:

$$f_V(\dot{l}_M) = 1 + \arctan(c_1(\dot{l}_M/V_{\max})^3 + c_2(\dot{l}_M/V_{\max})^2 + c_3(\dot{l}_M/V_{\max})) \quad \text{(A.5)}$$

TABLE V
NONSPECIFIC PARAMETERS OF PASSIVE ELEMENTS

Tendon (A.1)	**Parallel-Elastic Element (A.2)**	**Parallel-Viscous Element (A.3)**
σ_T [N/cm^2] = 1146	F_{PO} [N] = $0.129F_o$	k_D [Ns/m] = 20
$k_{\rm TE}$ [m^{-1}] = $43.478/l_{T0}$	F_o [N] = $\sigma_m A_m$	
k_T [N/m] = $1.2^*10^5 A_T/l_{T0}$	$k_{\rm PE} = 4.525/l_{M0}$	
$l_{TC} = 1.02 l_{T0}$		
F_C [N] = $\sigma_T A_T[e^{20/23} - 1]$		

where $V_{\max}$ is the maximum shortening velocity, and c_i $(i = 1, 2, 3)$ are curve-fitting constants taken from the literature [6]. It should be mentioned that the velocity-tension relationship of the muscle fiber is asymmetric about zero velocity [52].

3) Model Parameters: The proposed musculo-tendon model that is given in Fig. 2 includes two sets of parameters. One set includes the muscle-specific parameters, that are used to represent a particular muscle's (and tendon's) geometry of an individual subject, including: the musculo-tendon length $(l_{\rm MT})$, muscle fiber rest length (l_{M0}), the tendon rest length (l_{T0}), the muscle cross-sectional area (A_M), the tendon cross-sectional area (A_{TT}), and the muscle mass (m). The second set used nonspecific muscle parameters which were assumed to be the same for all the muscles. These parameters are associated with the nominal stress-strain curves of tendon and fascia [52].

In the present study the specific parameters were evaluated by using both *in vivo* and *in vitro* measurements. *In vivo* measurements that incorporate magnetic resonance imaging (MRI) were performed on the subject. MRI data were then used to estimate the following properties: 1) quadriceps mass, 2) cross-sectional area of the quadriceps muscle, and 3) musculo-tendon length [53]. In addition, we used data that were obtained via *in vitro* studies on cadavers to evaluate: 1) the musculo-tendon length of the quadriceps at a knee angle of 60°, while the hip is fixed at 90°, 2) the rest lengths of the quadriceps, and 3) the rest length of the quadriceps tendon. The *in vitro* obtained parameters were then scaled to fit the specific paraplegic subject by using the femur length and the circumference of the thigh at its half length region [6]. The specific parameters used in the above model for the subject referred to as Subject Vt, were as follows:

$m = 0.86$ [Kg] muscle mass, calculated as product of muscle's volume and density (=1.06 gr/cm^3).

$A_M = 19.7$ [cm^2] muscle cross-section area (evaluated by MRI).

$A_T = 0.56$ [cm^2] tendon cross-section area [6].

$l_{\rm MT} = 0.412$ [m] *in vivo* $l_{\rm MT}$ at knee angle of 0° while hip angle was fixed at 90° (evaluated by MRI).

$l_{\rm MTO} = C_{LMT} l_{\rm MT}$ muscle length at knee angle of 60° ($C_{LMT} = 0.935$, presents proportionality constant of slack $l_{\rm MT}$ versus $l_{\rm MT}$ *in vivo*, see [6]).

$l_{T0} = l_{\rm MTO} - l_{MO}\cos\alpha$ tendon slack length.

TABLE VI
LENGTH-TENSION AND VELOCITY-TENSION RELATIONSHIPS OF THE ACTIVATED MUSCLE FIBERS

Length-Tension (A.4)	$b_1 = -1.317$	$b_2 = -0.403$	$b_3 = 2.454$
Velocity-Tension (A.5)	$c_1 = -0.906$	$c_2 = 4.501$	$c_3 = -2.024$

l_{MO} muscle rest length, calculated as the non-trivial solution of

$$f_T(l_T) - f_{\rm PE}(l_M)\cos\alpha = 0$$

when setting $F_{\rm CE} = F_{\rm PV} = 0$.

The nonspecific parameters used in the above model to describe the length-tension and velocity-tension relationships of the muscle tendon and of the muscle passive elements are shown in Table V [6] where F_o is the maximal isometric force, which is the product of the muscle's specific tension and the physiological cross-sectional area (A_M).

The dimensionless curve-fitting constants that were used to describe the length-tension and velocity-tension relationships of the activated muscle fibers are shown in Table VI [6].

APPENDIX B
THE EXPRESSIONS FOR THE METABOLIC HISTORY FUNCTIONS

During interrupted stimulation, fatigue and recovery occur alternately. The histories of the above-mentioned metabolites must therefore be expressed in terms of two time-dependent metabolic functions. Our objectives were: 1) to construct a function that represents the intracellular levels of inorganic phosphates (Pi and $H_2PO_4^-$) and pH at any stage of interrupted functional electrical stimulation and 2) to determine the relation between the levels of these metabolites and the force generation capacity of the activated muscle. The metabolic data, used in the present study and acquired by the means of magnetic resonance spectroscopy (MRS), revealed a variation of the peak values of PCr and Pi and a chemical shift between these peaks [17], [46]. Intracellular pH was calculated using the following equation [21]:

$$\mathrm{pH}(\mu) = 6.75 + \log\left(\frac{\mu - 3.27}{5.96 - \mu}\right) \qquad \text{(B.1)}$$

where μ is the chemical shift in ppm of the Pi peak relative to the PCr peak.

During the fatigue phase of the muscle, the level of the metabolites varies according to the following functions:

$$x(t) = \begin{cases} \beta_{11} + \beta_{12}[1 + \beta_{13}\exp(-\beta_{14}t)]; & x(t) \equiv \mathrm{Pi}^F(t) \\ \beta_{21} + \beta_{22}\tanh[\beta_{23}(t - \beta_{24})]; & x(t) \equiv \mathrm{pH}^F(t). \end{cases} \tag{B.2}$$

The procedure used to evaluate the metabolic levels as given in (B.2) included least square curve fitting of Pi accumulation and pH decay with respect to time t (started from the onset of a 3 min-supra-maximal intensity contraction, applied on an initially unfatigued quadriceps muscle). $\beta_{11} - \beta_{14}$ (obtained by curve-fitting the Pi level versus time) and $\beta_{21} - \beta_{24}$ (pH obtained by curve-fitting pH level versus time) were considered to be constant parameters [6], [24].

During the rest period, the level of the metabolites vary according to the following functions:

$$x(t) = \begin{cases} \delta_{11} + \delta_{12}\exp(-\delta_{13}t); & x(t) \equiv \mathrm{Pi}^R(t) \\ \delta_{21} + \delta_{22}[1 - \exp(-\delta_{23}t)]; & x(t) \equiv \mathrm{pH}^R(t) \end{cases} \tag{B.3}$$

using the following sets of constant parameters: δ_{11}–δ_{13} (Pi versus time) and δ_{21}–δ_{23} (pH versus time). The procedure used to evaluate the metabolic levels as given in (B.3) was based on metabolic data, which were measured during a 45-min rest period that follows the 3 min, supra-maximal intensity, first-stimulation fatigue contraction. The curve-fitting constants which were used in (B.2) and (B.3) were as follows:

i) *Fatigue Metabolic History Constants (B.2)*

Pi History

$$\beta_{11}[\textit{dimensionless}] = 3.5059$$
$$\beta_{12}\ [\textit{dimensionless}] = 0.2278$$
$$\beta_{13}\ [\mathrm{sec}^{-1}] = -12.486$$
$$\beta_{14}\ [\mathrm{sec}] = 0.0294$$

pH History

$$\beta_{21}\ [\textit{dimensionless}] = 6.70$$
$$\beta_{22}\ [\textit{dimensionless}] = -0.502$$
$$\beta_{23}\ [\mathrm{sec}^{-1}] = 0.0406$$
$$\beta_{24}[\mathrm{sec}] = 30.0.$$

ii) *Recovery Metabolic History Constants (B.3)*

Pi History

$$\delta_{11} = \beta_{11} + \beta_{12} + \beta_{12}\beta_{13}$$
$$\delta_{12}\ [\textit{dimensionless}] = 2.23$$
$$\delta_{13}\ [\mathrm{sec}^{-1}] = 0.0070$$

pH History

$$\delta_{21} = \beta_{21} + \beta_{22}$$
$$\delta_{22} = \beta_{21} + \beta_{22}\tanh(-\beta_{23}\beta_{24}) - \delta_{21}$$
$$\delta_{23}\ [\mathrm{sec}^{-1}] = 0.0018.$$

The level of the monovalent phosphate ($H_2PO_4^-$) was calculated using the following expression [16]:

$$[\mathrm{H_2PO_4^-}] = \frac{[\mathrm{Pi}]}{(1 + (pK/[\mathrm{H^+}]))} \tag{B.4}$$

where pK $(=1.78E{-}7)$ is the equilibrium constant for mono—to divalent phosphoric acid, and $[H^+]$ is calculated from the intracellular pH. Subdividing (B.4) by its rest value $[H_2PO_4^-]_o$, the metabolic history of $H_2PO_4^-$ follows:

$$x(t) = \frac{1 + (pK/y_{\mathrm{pH}_o})}{(1 + (pK/y_{\mathrm{pH}}(t))}\, y_{\mathrm{Pi}}(t) \tag{B.5}$$

and

$$y_{\mathrm{pH}}(t) = 10^{-\mathrm{pH}(t)} \tag{B.6}$$

where $y_{\mathrm{Pi}}(t)$ expresses the temporal level of Pi normalized to its rest value as obtained from (B.2), $y_{\mathrm{pH}}(t)$ is the calculated intracellular concentration of $[H^+]$, and $y_{\mathrm{pH}o}$ is the rest value of $y_{\mathrm{pH}}(t)$.

REFERENCES

[1] A. Kralj and T. Bajd, *Functional Electrical Stimulation: Standing and Walking after Spinal Cord Injury*. CRC, Boca Raton, FL, 1989.

[2] J. Mizrahi, "Fatigue in muscles activity by functional electrical stimulation," *Crit. Rev. Phys. Rehab. Med.*, vol. 9, pp. 93–129, 1997.

[3] M. Levy, J. Mizrahi, and Z. Susak, "Recruitment, force and fatigue characteristics of quadriceps muscle of paraplegics isometrically activated by surface functional electrical stimulation," *J. Biomed. Eng.*, vol. 12: pp. 150–156, 1990.

[4] J. Mizrahi, O. Levin, A. Aviram, E. Isakov, and Z. Susak, "Muscle fatigue in interrupted stimulation: Effect of partial recovery on force and EMG dynamics," *J. Electromyogr. Kinesiol.*, vol. 7, pp. 51–65, 1997.

[5] B. D. Popovic, "Functional electrical stimulation for lower extremities," in *Neural Prostheses: Replacing Motor Function after Disease or Disability*, R. B. Stein, P. H. Peckham, and B. D. Popovic, Eds. New York: Oxford University Press, 1992, pp. 233–251.

[6] Y. Giat, J. Mizrahi, and M. Levy, "A musculotendon model of the fatigue profiles of paralyzed quadriceps muscle under FES," *IEEE Trans. Biomed. Eng.*, vol. 40, pp. 664–674, 1993.

[7] A. Kralj, T. Bajd, R. Turk, and H. Benko, "Posture switching for prolonging functional electrical stimulation standing in paraplegic patients," *Paraplegia*, vol. 24, pp. 221–230, 1986.

[8] H. B. K. Boom, A. J. Mulder, and P. H. Veltink, "Fatigue during functional electrical neuromuscular stimulation," in *Progress in Brain Research*, J. H. J. Allum, D. J. Allum-Mechlenburg, P. F. Harris, and R. Probst, Eds. Amsterdam, The Netherlands: Elsevier Science, 1993, vol. 97, pp. 409–418.

[9] R. H. T. Edwards, "Human muscle function and fatigue," in *Human Muscle Fatigue: Physiological Mechanisms*, R. Proter and J. Whelan, Eds. London, U.K.: Pitman Medical, 1981, pp. 1–18.

[10] R. H. Fitts, "Cellular mechanisms of muscle fatigue," *Physiol. Rev.*, vol. 74, pp. 49–94, 1994.

[11] E. Kugelberg and B. Lindegren, "Transmission and contraction fatigue of rat motor units in relation to succinate dehydrogenase activity of motor unit fibers," *J. Physiol. (London)*, vol. 288, pp. 285–300, 1979.

[12] B. Bigland-Ritchie and J. J. Woods, "Changes in muscle contractile properties and neural control during human muscular fatigue," *Muscle Nerve*, vol. 7, pp. 690–699, 1984.

[13] G. C. Sieck and Y. S. Prakash, "Fatigue at the neuromuscular junction," in *Neural and Muscular Mechanisms, Advanc.*, S. C. Gandevia, R. M. Enoka, A. J. McComas, D. G. Stuart, and C. K. Thomas. Eds. *Experi. Med. Biol.*, vol. 384, pp. 83–100, 1995.

[14] Z. Susak, M. Levy, E. Isakov, and J. Mizrahi, "The duration of isometric contraction while using FES with stimuli of different parameters," in *Proc. 2nd Vienna Int. Workshop Functional Electrostim.*, Vienna, Austria, 1986, pp. 75–78.

[15] G. Sjogaard and A. J. McComas, "Role of interstitial potassium," in *Fatigue: Neural and Muscular Mechanisms, Advanc.*, S. C. Gandevia, R. M. Enoka, A. J. McComas, D. G. Stuart, and C. K. Thomas, Eds., *Experi. Med. Biol.*, vol. 384, pp. 69–80, 1995.

[16] M. Degroot, B. M. Massie, M. Boska, J. Gober, R. G. Miller, and W. Weiner, "Dissociation of [H^+] from fatigue in human muscle detected by high time resolution ^{31}P NMR," *Muscle Nerve*, vol. 16, pp. 91–98, 1993.
[17] M. Levy, T. Kushnir, J. Mizrahi, and Y. Itzchak, "In-vivo ^{31}P NMR studies of paraplegics' muscles activated by functional electrical stimulation," *Magnet. Reson. Med.*, vol. 29, pp. 53–58, 1993.
[18] A. J. Baker, P. J. Carson, R. G. Miller, and M. W. Weiner, "Metabolic and nonmetabolic components of fatigue monitored with ^{31}P-NMR," *Muscle Nerve.*, vol. 17, pp. 1002–1009, 1994.
[19] P. Vestergaard-Poulsen, C. Thomsen, T. Sinkjaer, and O. Henriksen, "Simultaneous ^{31}P NMR spectroscopy and EMG in exercising and recovering human skeletal muscle—A correlation study," *J. Appl. Physiol.*, vol. 97, pp. 1469–1478, 1995.
[20] D. L. Arnold, P. M. Matthews, and G. K. Radda, "Metabolic recovery after exercise and the assessment of mitochondrial function *in-vivo* in human skeletal muscle by means of ^{31}P NMR," *Mag. Reson. Med.*, vol. 1, pp. 307–315, 1984.
[21] D. J. Taylor, P. Styles, P. M. Matthews, D. A. Arnold, D. G. Gadian, P. Bore, and G. K. Radda, "Energetics of human muscle: Exercise-induced ATP depletion," *Magnet. Reson. Med.*, vol. 3, pp. 44–54, 1986.
[22] R. G. Miller, D. Giannini, H. S. Milner-Brown, R. B. Layzer, A. P. Koretsky, D. Hooper, and M. W. Weiner, "Effects of fatiguing exercise on high-energy phosphates, force, and EMG: Evidence for three phases of recovery," *Muscle Nerve*, vol. 10, pp. 810–821, 1987.
[23] P. Vestergaard-Poulsen, C. Thomsen, J. Norregaard, P. Bulow, T. Sinkjaer, and O. Henriksen, "^{31}P NMR spectroscopy and EMG during exercise and recovery in patients with fibromyalgia," *J. Rheumatol.*, vol. 22, pp. 1544–1551, 1995.
[24] Y. Giat, J. Mizrahi, and M. Levy, "A model of fatigue and recovery in paraplegic's quadriceps muscle subjected to intermittent FES," *ASME J. Biomed. Eng.*, vol. 118, pp. 357–366, 1996.
[25] C. Juel, "Potassium and sodium shift *in-vivo* isometric contraction, and time courses of ion-gradient recovery," *Pflugers Arch.*, vol. 406, pp. 458–463, 1986.
[26] J. Mizrahi, M. Levy, H. Ring, E. Isakov, and A. Liberson, "EMG as an indicator of fatigue in isometrically FES-activated paralyzed muscles," *IEEE Trans. Rehab. Eng.*, vol. 2, pp. 57–65, 1994.
[27] J. He, W. S. Levine, and G. E. Loeb, "Feedback gains for correcting small perturbations to standing posture," *IEEE Trans. Automat. Contr.*, vol. 36, pp. 322–332, 1991.
[28] M. G. Hoy, F. E. Zajac, and M. E. Gorgon, "A musculoskeletal model of the human lower extremity: The effects of muscle, tendon, and moment arm on the moment-angle relationship of musculotendon actuators at the hip, knee, and ankle," *J. Biomech.*, vol. 23, pp. 157–169, 1990.
[29] M. R. Enoka, *Neuromechanical Basis of Kinesiology*, 2nd Edition. Champaign IL: Human Kinetic, p. 216, 1994.
[30] S. Salmons and F. A. Sreter, "Significance of impulse activity in the transformation of skeletal muscle type," *Nature*, vol. 263, pp. 30–34, 1976.
[31] S. Ebashi and M. Endo, "Calcium ion and muscle contraction," *Progr. Biophys. Molec. Biol.*, vol. 18, pp. 123–183, 1968.
[32] T. Sinkjaer, N. Gantchev, and L. Arendt-Nielsen, "Mechanical properties of human ankle extensors after muscle potentiation," *Electroenceph. Clin. Neurophysiol.*, vol. 85, pp. 412–418, 1992.
[33] T. G. Sandercock, J. A. Faulkner, J. W. Albers, and P. H. Albrecht, "Single motor unit and fiber action potential during fatigue," *J. Appl. Physiol.*, vol. 58, pp. 1073–1079, 1985.
[34] C. Juel, "Muscle action potential propagation velocity changes during activity," *Muscle Nerve*, vol. 11, pp. 714–719, 1988.
[35] R. E. Burke, D. N. Levine, P. Tsairis, and F. E. Zajac, "Physiological types and histochemical profiles in motor units of the cat gastrocnemius," *J. Physiol. (London)*, vol. 234, pp. 723–748, 1973.
[36] D. G. Moiescu, "Kinetics of reaction in calcium-activated skinned muscle fibers," *Nature*, vol. 262, pp. 610–613, 1976.
[37] M. B. Cannell and D. Allen, "Model of calcium movements during activation in the sarcomer of frog skeletal muscle," *Biophys. J.*, vol. 45, pp. 913–925, 1984.
[38] R. B. Stein, J. Bobet, M. N. Oguztoreli, and M. Fryer, "The kinetics relating calcium and force in skeletal muscle," *Biophys. J.*, vol. 54, pp. 705–717, 1988.
[39] G. I. Zahalak and S.-P. Ma, "Muscle activation and contraction: Constitutive regulation based directly on cross-bridge kinetics," *ASME J. Biomed. Eng.*, vol. 112, pp. 52–62, 1990.
[40] J. R. Blinks, R. Rudel, and S. R. Taylor, "Calcium transients in isolated amphibian skeletal muscle fibers: Detection with aeqorin," *J. Physiol. (London)*, vol. 277, pp. 291–323, 1977.
[41] S-P. Ma and G. I. Zahalak, "A distribution-moment model of energetics in skeletal muscle," *J. Biomech.*, vol. 24, pp. 21–35, 1991.
[42] D. G. Stephenson and D. A. Williams, "Calcium-activated force reaponses in fast-and slow-twitch skinned muscle of the rat at different temperatures," *J. Physiol. (Lond.)*, vol. 317, pp. 284–302, 1981.
[43] Y. Giat, "Prediction of muscular synergism and antagonism of human upper extremity—A dynamic optimization approach," Ph.D. dissertation, Univ. Maryland, 1990.
[44] D. H. Haynes and A. Mandveno, "Computer Modeling of Ca^{+2} pump function of Ca^{+2}-Mg^{+2}-ATPase of sarcoplasmic reticulum," *Physiol. Rev.*, vol. 67, pp. 244–284, 1987.
[45] J. Minzly, J. Mizrahi, E. Isakov, Z. Susak, and M. Verbeke, "Computer-controlled portable stimulator for paraplegic patients," *J. Biomed. Eng.*, vol. 15, pp. 333–338, 1993.
[46] M. Levy, "Fatigue of paralyzed skeletal muscle activated in-vivo by electrical stimulation," D.Sc. dissertation, Technion—Israel Inst. Technol., Israel, 1990.
[47] T. Yoshida, H. Watari, and K. Tagawa, "Effects of active and passive recoveries on splitting of the inorganic phosphate peak determined by ^{31}P-nuclear magnetic resonance spectroscopy," *NMR Biomed.*, vol. 9, pp. 13–19, 1996.
[48] J. Mizrahi, D. Seelenfreund, E. Isakov, and Z. Susak, "Predicted and measured force after recovery of differing duration following fatigue in FES," *Artif. Organs*, vol. 21, pp. 236–239, 1997.
[49] L. Lindstrom and R. Magnusson, "Interpretation of myoelectric power spectra: A model and its applications," in *Proc. IEEE*, 1977, vol. 65, pp. 653–662.
[50] R. Merletti, M. Knaflitz, and C. J. DeLuca, "Electrically evoked myoelectric signals," *Crit. Rev. Biomed. Eng.*, vol. 19, pp. 293–340, 1992.
[51] R. Merletti, "Interpretation of fatigue plots during electrically elicited isometric muscle contraction," *World Congr. Med. Phys. Biomed. Eng.*, Nice, France, p. 50, Sept. 14–19, 1997.
[52] F. Z. Zajac, "Muscle and tendon: Properties, models, scaling, and application to biomechanics and motor control," *CRC Biomed. Eng.*, vol. 17, pp. 359–411, 1989.
[53] O. Levin, "Characterization of force dynamics of a paralyzed muscle activated by electrical stimulation," Ph.D. dissertation, Technion—Israel Inst. Technol., Israel, 1998.

Oron Levin received the B.Sc. degree in physics from the Ben-Gurion University of the Negev, Beer-Sheva, in 1990, the M.Sc. and Ph.D. degrees in biomechanics from the Technion—Israel Institute of Technology, Haifa, in 1994 and 1998, respectively.

In 1998, he has joined the Department of Rehabilitation Sciences, Hong-Kong Polytechnic University, Hong-Kong, as a Research Fellow. His research interests are in the modeling of the musculoskeletal system and functional electrical stimulation of muscles.

Joseph Mizrahi received the B.Sc. degree in aeronautical engineering in 1967, the M.Sc. degree in mechanics in 1970 and the D.Sc. degree in biomechanics in 1975 all from the Technion—Israel Institute of Technology, Haifa.

He is a Professor of Biomechanics at the Department of Biomedical Engineering, Technion—Israel Institute of Technology, and during the academic year 1998–1999, he is on sabbatical with the Department of Rehabilitation Sciences, the Polytechnic University in Hong Kong. He has been Head of the Biomechanics Laboratory at the Loewenstein Rehabilitation Center in Israel for 18 years. He has also held various visiting positions, including in Harvard Medical School, where he spent the 1989–1990 academic year. He has been the principal author of about 185 publications, including papers, book chapters, and conference proceedings. His major research interests and publications are in orthopaedic biomechanics and rehabilitation biomechatronics.